Trap states in ZnPc:C60 small-molecule organic solar cells

Lorenzo Burtone, Janine Fischer, Karl Leo, and Moritz Riede
Institut für Angewandte Photophysik, Technische Universität Dresden, D-01062 Dresden, Germany
(Received 12 September 2012; published 31 January 2013)

Trap states are known to be one of the key parameters limiting charge transport in organic semiconductors and hence the performance of organic solar cells. Here, small-molecule organic solar cells based on a bulk heterojunction between zinc-phtalocyanine (ZnPc) and the fullerene C60 are characterized according to their trapping nature by noninvasive methods and under ambient conditions. We show how impedance spectroscopy, applied to systematically varied device structures, reveals the trap localization as well as its occupation mechanisms. Further insight is given from investigations of different device working points and illumination intensities. Thus, we find the traps to be bulk states in the active layer with an electron-trapping nature. They can be described by a Gaussian energy distribution of 55 meV width, centered at 0.46 eV below the electron transport level and with a concentration of 3.5×10^{16} cm^{-3}. Moreover, the trap states act as recombination centers in the presence of injected or photogenerated charge carriers. The results are confirmed by electrical simulations.

DOI: 10.1103/PhysRevB.87.045432 PACS number(s): 72.20.Jv, 73.61.Ph

I. INTRODUCTION

The investigation of trap states is an important aspect in organic semiconductor research and the electrical characterization of the traps is essential for a correct understanding and simulation of organic devices.[1–7] Although the known contribution of trap states in the device behavior, a reliable characterization technique of defects is still not available for organic semiconductors. Most of the methods known from inorganic semiconductors are not easily applicable to the organic materials because of the fundamental differences in the charge carrier transport mechanism. One such approach is deep-level transient spectroscopy (DLTS), which has been applied to organic semiconductors.[8,9] However, the wide measurement temperature range required by this technique renders it suitable only for a limited number of materials in which the variation of transport properties with temperature either does not significantly affect the results or can be described by theoretical models.[10,11] Additionally, the abundance of trap states can cause a symmetry in trapping and detrapping times and one of the assumptions in DLTS is that a trapping process is faster than detrapping, a requirement usually fulfilled in crystalline materials.[12] Other methods such as time-resolved infrared (TRIR) spectroscopy[13] or thermally stimulated current (TSC) have also been applied with promising results.[14,15] However, TRIR spectroscopy requires semiconductors with a suitable infrared absorption and TSC presents the same temperature-related problems of DLTS. In particular, TRIR uses the sensitivity of vibration modes to the charge distribution and requires materials with a small absorption cross section of polarons in the spectral region of the analyzed vibration modes. In TSC the trapped charge carriers are released by heating up the sample and the current is recorded as a function of temperature. In this technique the current is determined by both the thermal release of trapped charge carriers and the temperature dependence of the mobility. The temperature dependence of the mobility is usually neglected, but this assumption is not always acceptable for organic semiconductors.

In our contribution we employ impedance spectroscopy (IS) to characterize the trap states in small molecule solar cells.[16,17] This technique presents a number of advantages. Firstly, it is a steady-state measurement. Therefore, the trap response can be described with small-signal models and analyzed at different device working points. The response dynamics is analyzed in the frequency domain enabling effective distinction of the contributions from processes with different characteristic time constants. Secondly, the measurement is noninvasive and can be performed on complete and working devices. This is an important aspect because the morphological and electronic properties of a pristine organic material can be drastically different if mixed with dopants or other materials, as in the case of a blend active layer.[18,19] Defects are furthermore not only correlated with the materials used, but also with the specific device structure and fabrication conditions. Therefore, the analysis of pristine materials is not always exhaustive.

Recent publications reported the presence of trap states in small-molecule solar cells by analyzing the capacitance spectra of the devices.[17,20,21] In these contributions, it was shown that the capacitive contribution of trap states was significant in the low-frequency range, where the trapped charges were able to follow the probe signal. For higher frequencies, only the dielectric response of the intrinsic materials contributed to the device capacitance. In this work, the characteristics of the trap states are analyzed in more detail: their spatial distribution, the trapping-detrapping mechanism, the energy distribution of defect states and their role as recombination centers are discussed. To access this information, the structure of the device, the internal field, and the photogenerated charge carrier density are systematically modified by measuring solar cells of different thicknesses at varying bias voltage or light intensity. In order to have a quantitative estimation about the energetic distribution of trap states, electrical simulations are employed to estimate the energy diagram of the device. Subsequently, the capacitance spectrum of the solar cells is calculated for different trap distributions and compared with the measured data.

II. METHODS

A. Experimental

The investigated devices are solar cells with an active layer composed by a blend bulk-heterojunction of

 ©2013 American Physical Society

zinc-phthalocyanine (ZnPc, TCI Europe) as donor material and the fullerene C60 (CreaPhys GmbH) as acceptor, co-evaporated in a 1:1 volume ratio. Both materials are purified at least twice by vacuum gradient sublimation. The solar cells based on the p-i-n concept[22–24] present transport layers made of n-doped C60 for the electrons and p-doped N, N, N', N'-tetrakis(4-methoxyphenyl)-benzidine (MeO-TPD, Sensient) for the holes. The n-dopant[25] molecule is a tungsten dimetal complex $W_2(hpp)_4$ from Novaled AG, while for p-doping[26] C60F36 from MTR Ltd. is used. The devices are evaporated on a glass/indium tin oxide (ITO) substrate from Thin Film Devices, USA and the active area, defined as the geometric overlap between ITO and Al, is 6.44 mm^2. The encapsulation is performed in nitrogen atmosphere and consists of a cover glass sealed with a UV-curing epoxy (Nagase).[27]

The capacitance measurements are performed at room temperature with an Autolab PGSTAT302N. The probe signal is superimposed to a constant bias voltage and has an amplitude of 15 mV(rms). The frequency is varied from 10 Hz to 1 MHz. Illumination is provided by white LEDs (LUXEON® K2 Star Natural White, from Philips Lumileds) and reaches an irradiance of 800 mW/cm^2. The device capacitance is calculated from the imaginary part of the admittance as

$$C(\omega) = \frac{\Im[Y(\omega)]}{\omega} \tag{1}$$

where $Y(\omega)$ is the complex admittance and ω is the angular frequency.[28]

B. Device modeling

For the description and fitting of the experimental data, a combination of equivalent circuit and drift-diffusion simulations is applied. The equivalent circuit approach is preferred for a first description of the device behavior being aware of the necessity to assign physical meaning to the equivalent circuit elements used for fitting.

In the case of organic solar cells, the device can be described, in a first approximation, by the equivalent circuit of Fig. 1(a). The series resistance R_s takes into account the effect of contacts and transport layers, whereas the parallel capacitance C_p represents the geometrical and chemical capacitance of the intrinsic layer. The parallel resistance R_p supports the current flowing through the device. In this approach, the physical meaning of the parallel capacitance is given by the field drop over the intrinsic materials, similar to a parallel plate capacitor. In presence of a significant charge carrier accumulation in the intrinsic layer (due to light absorption or charge carrier injection), the parallel capacitance has an additional contribution described by a chemical capacitance.[29,30] The parallel resistance involves more complicated physical mechanisms, however in a first approximation it describes the recombination process taking place when charge carriers are injected into the blend layer, in forward bias.[31]

In presence of trap states an additional contribution to the electrical response of the device is observed. The charge carriers can be trapped and stored in intragap states, influencing the transport and the field distribution in the solar cell. The equivalent circuit of one discrete trap level in the gap of a semiconducting device was already investigated by Losee.[33] In his model, the energy loss of trapped charge carriers was described by a resistive element R_{trap}, while the density of trapped charges gave the capacitive contribution C_{trap}. The overall equivalent circuit was therefore the same as in Fig. 1(a) with the additional trap contribution and is depicted in Fig. 1(b). The equivalent circuit proposed by Losee has the advantage of describing the response of trap states in a simple way and without introducing an high number of fitting parameters. However, in organic semiconductors the description of traps with one discrete intragap level is not realistic and a more sophisticated distribution of trap states is

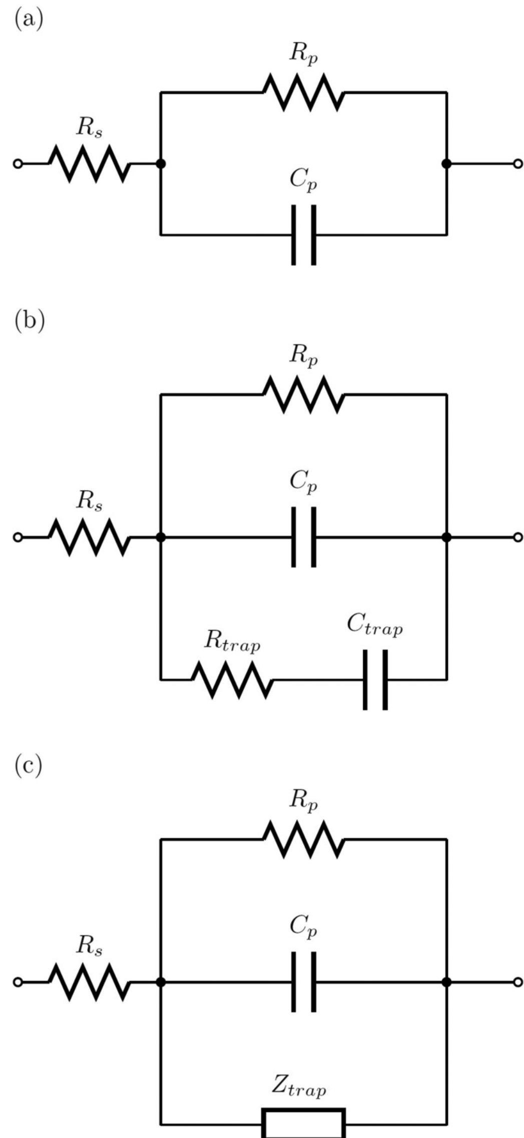

FIG. 1. Small-signal equivalent circuits for organic solar cells. The circuit (a) describes an ideal device, without trap states, and is composed of one series resistance R_s, one parallel resistance R_p and one parallel capacitance C_p. In circuit (b) the trap states are described with the Losee model, considering one discrete effective intragap level modeled by one trap resistance R_{trap} and one trap capacitance C_{trap}. In a more general approach, the trap impedance is a complex function derived from the specific distribution of intragap states Z_{trap}, as in circuit (c).

necessary.[17] In general, the impedance of the circuital element for trap states can be complicated, but the structure of the overall equivalent circuit is preserved. In the general case, the impedance of the trap element Z_{trap} is derived from the small signal approximation of the physical model of the solar cell, as shown in Fig. 1(c).

In this work, the trap impedance is calculated starting from a small-signal model developed for dye-sensitized solar cells (DSCs),[34] where an exponential distribution of trap states is present. This analytical model is generalized to describe a generic distribution $g(E)$ of trap states and the details of the model derivation are reported in the Supplemental Material.[32] With the hypothesis of one single transport level and assuming Boltzmann statistics with instantaneous response of the free charges to the modulation signal, the capacitance function can be expressed as

$$Z_{trap}(\omega)^{-1} = Y_{trap}(\omega) = j\omega \frac{q^2}{k_B T} \int_{E_g} \frac{g(E) f_t(E)[1 - f_t(E)]}{1 + j\omega/\omega_t} dE. \quad (2)$$

Here q is the elementary charge, k_B the Boltzmann constant, T the temperature, and the integration interval is the energy gap E_g. The trap states are defined by the characteristic trapping-detrapping frequency ω_t,[34,35] the state distribution function $f_t(E)$, and their energy distribution $g(E)$. To solve this integral it is necessary to define the position of the Fermi level with respect to the transport level at every position of the device structure, i.e., knowing the energy diagram. From the energy diagram, it is possible to estimate the DOS of the trap states from the capacitance spectra of the solar cells.

The equivalent circuit applied to fit the experimental impedance spectra is shown in Fig. 1(c), where the trap impedance Z_{trap} is given by Eq. (2). The values of the series and parallel resistances R_s and R_p are at first estimated by graphical inspection of the impedance modulus at high and low frequencies, respectively, and then obtained from a complex nonlinear least square (CNLS) fitting procedure[36] (see Supplemental Material).[32] The parallel capacitance is calculated as the geometrical capacitance of the intrinsic blend layer, using a relative static permittivity of $\varepsilon = 4.7$ (estimated in house by independent capacitance measurements).

For information about the energy diagram of the device, drift-diffusion simulations are performed, which are explained in the following. The drift-diffusion model describes band transport of electrons and holes by the equations for continuity and diffusion as well as Poisson's equation for the electrical coupling. This differential equation system is numerically solved assuming a Boltzmann distribution for the occupation statistics. Details on the simulations can also be found in the work from Tress[37] showing its successful application to the device modeling of organic solar cells. Here, we assume ohmic contacts, bimolecular recombination according to modified Langevin theory,[38] and constant charge carrier mobilities in the intrinsic layer ($\mu_n = 10^{-8}$ m^2/Vs, $\mu_p = 5 \times 10^{-9}$ m^2/Vs). A Gaussian distribution of electron trap states is used, given by

$$g(E) = \frac{N_t}{\sqrt{2\pi}\sigma} \exp \frac{(E_t - E)^2}{2\sigma^2}, \quad (3)$$

where N_t is the concentration of trap states, σ the width of the energetic distribution and E_t the energy of the Gaussian peak. This distribution is used to describe the static trap density,

$$n_t = \int g(E) f(E) dE \quad (4)$$

with $f(E)$ being the Fermi distribution. Furthermore, trap states are considered as additional recombination centers causing current drain.[39] In this case, equal trapping rates for electrons and holes are assumed ($c_t = 2 \times 10^{-17}$ s^{-1}) and the trap level is set to the maximum of the Gaussian trap distribution E_t.

The energy diagram is first calculated without trap states and used to fit the capacitance spectra. The fit revealed a first estimation of the trap distribution, which was subsequently introduced into a second simulation in form of a Gaussian distribution. The presence of traps does not significantly influence the energy diagram as long as the trap concentrations is not significantly higher than 10^{17} cm^{-3} (see also Supplemental Material).[32]

III. RESULTS AND DISCUSSION

A. Variation of active layer thickness

To decide whether interface or bulk traps are present in the investigated solar cells, the thickness of the intrinsic active layer is varied between 40 nm and 100 nm. In Fig. 2, the capacitance spectra of three solar cells with different active layer thickness are depicted ($x = 40$ nm, 70 nm, and 100 nm). These measurements are performed in dark at 0V bias voltage. In the frequency range between 10 kHz and 100 kHz a first plateau is visible. The value of the capacitance in this spectral region corresponds to the geometrical capacitance of the intrinsic active layer and scales with the thickness like a plane capacitor ($C = \varepsilon \times$ *Area*/*intrinsic layer thickness*). The additional capacitive contribution of trap states is visible for frequencies lower than 1 kHz and results to be thickness independent over a significant range (see the inset of Fig. 2).

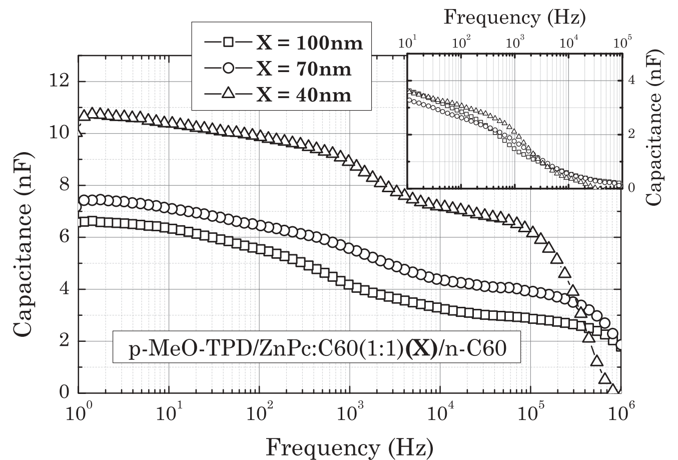

FIG. 2. Measured capacitance spectra of p-i-n small-molecule solar cells with varied active layer thickness. In the inset, the geometrical capacitance is subtracted from the spectra to isolate the trap contribution at frequencies below 10 kHz.

The results of Fig. 2 lead to two conclusions. First, traps give a capacitive contribution that is added to the geometrical capacitance. In terms of equivalent circuit this means that the trap capacitance is in parallel to the geometrical capacitance and is therefore given by traps located in the intrinsic layer and not in the doped transport layers. This conclusion is in agreement with previous observations.[17,20] It is justified by the high charge carrier density in the doped layers that increases the conductivity and fills the eventual traps, allowing for trap-free transport.[40] A second conclusion arising from the results of Fig. 2 is deduced by the thickness independence of the trap capacitance (inset of Fig. 2). This is a clear indication that the trap states responding to the signal are located at or close to an interface, eventually extended into the bulk for less then the 40 nm of the thinnest measured device. This seems to be in disagreement with the results present in literature,[20] where bulk traps were observed in presence of photogenerated charges. There, it was shown that trap states cannot contribute to the capacitance in dark, because no free charges were present in the blend intrinsic layer. When light was absorbed, free charge carriers were photogenerated and the trap states became populated and contributed to the device response. This is no contradiction to the results of Fig. 2 when only the *responding* traps are located in the proximity of an interface. It does not disprove the presence of trap states everywhere in the bulk active layer since they can be empty and do not give any contribution. This argumentation is better clarified by the effects produced varying the bias voltage and the illumination conditions.

B. Effect of doped transport layers

The second variation in the device structure involves the doped transport layers. It was discussed before that trap states have to be populated in order to contribute to the device capacitance. In the absence of doped layers, as long as no charge carriers are photogenerated, no trap capacitance is observed.[20] On the other hand, in presence of doped transport layers, the trap capacitance is present also in dark,[17] suggesting trap population by the doped transport layers. Four solar cells with different transport layers are measured. The first device is completely intrinsic, with a 50 nm thick blend ZnPc:C60 layer and without doped transport layers. The second solar cell has an additional p-doped hole transport layer, while the third one is a complete p-i-n stack. In order to further investigate the effect of dopant molecules in the trap states, another device is produced with one p-doped transport layer and 2 nm of pristine n-dopant between the intrinsic blend and the Al contact. The results are presented in Fig. 3. The measured current-voltage characteristics of the solar cells are shown in the Supplemental Material.[32]

The devices without a n-doped electron transport layer do not show any capacitive contribution of trap states at low frequency, while in presence of an n-doped ETL the traps are able to respond to the probe signal. The presence of trap states induced by the n-dopant molecules can be excluded observing the capacitance spectra of the device with 2 nm of pristine n-dopant between the intrinsic layer and the metal contact. The effect of this thin layer is to improve the ohmic properties of the Al contact[41,42] without introducing trap states in the intrinsic layer. Trap states are therefore electron trapping and can be populated by the free charges present in n-doped

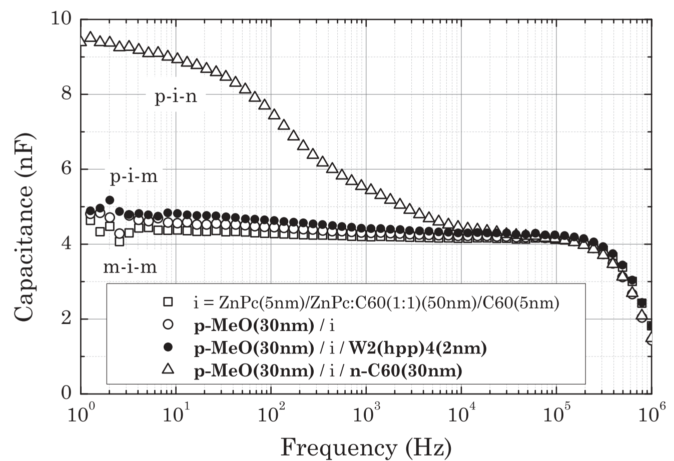

FIG. 3. Measured capacitance spectra of solar cells with different transport layers, the device structure are summarized in the legend. The trap states are responding only in presence of an n-doped electron transport layer (△).

C60. This mechanism is schematically depicted in Fig. 4. The strong charge carrier concentration gradient between intrinsic and doped layers induces a diffusion of charge carriers from the transport layers into the active layer. The built-in field that drops over the intrinsic layer prevents these free carriers from being injected. In the ideal case, very few free carriers effectively diffuse into the intrinsic layer and the traps stay empty, as in the case of devices without doped layers. However, close to the interface between doped and undoped materials, the trap states have an energy lower than the transport levels in the doped material and the field is not able to release these trapped charges. The proposed mechanism explains the results of Figs. 2 and 3, but is also in perfect agreement with the observations presented in literature.[17,20]

C. Trap distribution from simulations

In the following we focus on the 100 nm p-i-n solar cell, but the same results are obtained for different thicknesses, as shown in the Supplemental Material.[32] The discussed trapping mechanism is subsequently confirmed by electrical simulations and measurements under different bias and illumination conditions.

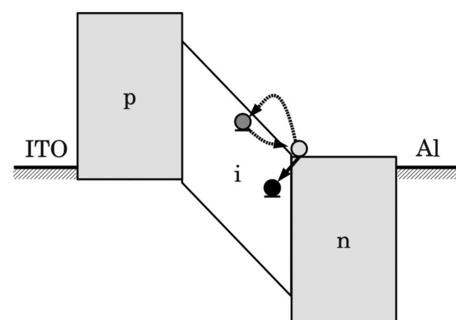

FIG. 4. Trap population mechanism. The charge carriers trapped in the intrinsic layer can be released by the field and accumulated in the doped transport layer. Close to the interface, the energy of trapped charges is below the transport level in the doped layer and the field-induced detrapping is prevented.

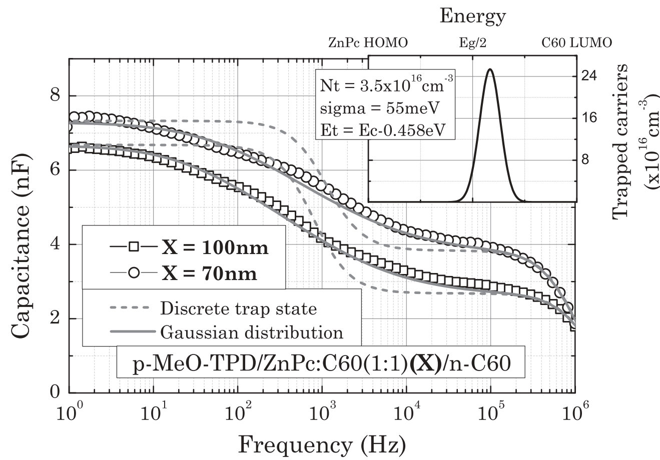

FIG. 5. Capacitance spectra of solar cells with two different intrinsic layer thicknesses. Measured data (symbols) are compared to simulated impedance data using the equivalent circuit of on single intragap level (dashed line) and employing a Gaussian trap distribution (solid line). The parameters of the Gaussian distribution are summarized in the inset.

The characterization of the trap states is obtained from the capacitance spectra using Eq. (2). Figure 5 shows the impedance spectra fitted with different trap distributions. The single-state model from Losee does not reproduce the measured data correctly. The best fit is obtained with a Gaussian distribution of trap states given by Eq. (3). In Fig. 5 the capacitance spectra are shown, while the fitting is performed on the complex impedance function (see Supplemental Material[32] for the impedance modulus spectra). The Gaussian is centered at $E_t = 0.458$ eV below the transport level of C_{60} and has a width of $\sigma = 55$ meV. The concentration of trap states results to be $N_t = 3.5 \times 10^{16}$ cm^{-3}, which is in the range of previously reported values.[16,17]

The current-voltage characteristics of the solar cells with different blend layer thicknesses are shown in Fig. 6 together with the drift-diffusion simulation results including the Gaussian trap distribution. The good agreement between

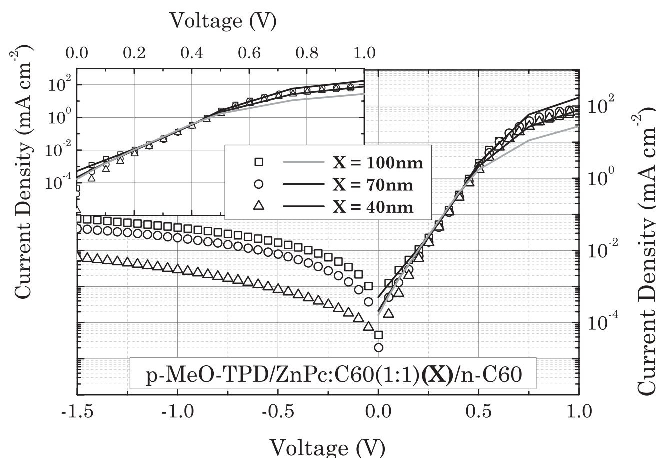

FIG. 6. J-V curves from experiment (symbols) and drift-diffusion simulations (solid lines) for three different thicknesses of the intrinsic layer. Inset: Zoom view of the exponential region showing a good agreement between experimental and simulation data.

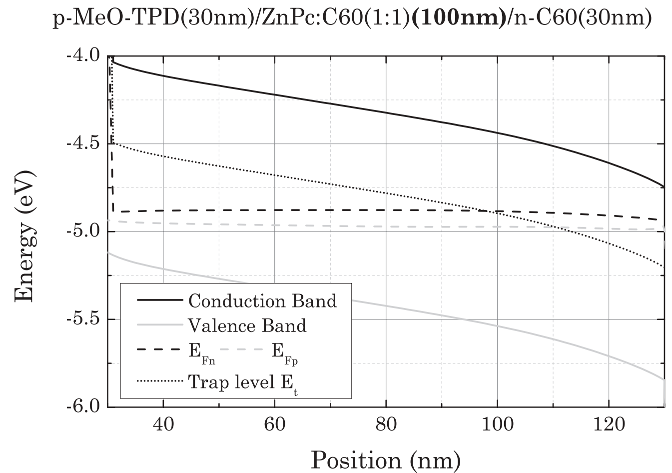

FIG. 7. Energy diagram at short circuit ($V_{\text{bias}} = 0$ V) resulting from drift-diffusion simulations of a p-i-n device with 100 nm thick intrinsic layer. The two quasi-Fermi levels for electrons and holes are shown in dashed lines. The energetic level of the peak of the Gaussian trap states distribution is plotted with a fine dotted line. For the sake of clarity, the x axis is confined to the intrinsic layer, between 30 nm and 130 nm. These results are obtained employing the Gaussian trap distribution estimated from the impedance spectra analysis of Fig. 5

measurements and calculations in the forward bias region confirms the validity of the implemented model. The ideality factor in the exponential region is close to 2 for all the solar cells, indicating a current dominated by trap-assisted recombination in the blend layer,[43] as it can be expected for heterostructures with doped transport layers, which introduce a barrier for minority carrier extraction. The correct description of the exponential part of the J-V characteristic is crucial for the validation of the energy diagram used to fit the capacitance spectra (Fig. 7), since the IS measurements are mostly performed in this region, at short circuit or with low current flowing. For bias voltage higher than approximately 0.7 V, a discrepancy between experimental data and simulations is observed. This is due to the effect of series and contact resistance, which limits the measured current independently from the intrinsic layer thickness. This effect is not considered in the simulations, where the current is limited by the resistance of the intrinsic layer, which is thickness dependent.

The energy diagram supports the idea of homogeneously distributed bulk traps that are populated only in the vicinity of the n-doped layer because the trap level is below the Fermi level in this region.

D. Response to the bias voltage

In IS, the small sinusoidal signal is superimposed to a constant bias voltage. By varying this bias voltage it is possible to analyze the device response in different working points. A change in the external bias results in a variation of the internal field.

According to the trap occupation mechanism of Fig. 4, the trapped charges can be more easily extracted from the intrinsic layer as the intensity of the internal field increases. Subsequently, the intensity of the capacitive contribution at low frequencies decreases. This behavior is shown in Fig. 8. It

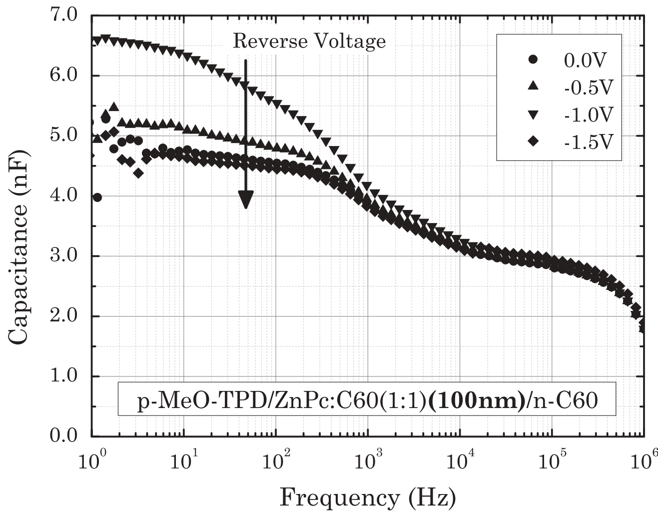

FIG. 8. Measured capacitance spectra of solar cells under different reverse bias voltages. The traps capacitance decreases with the reverse bias, due to the increasing extraction field in the active layer.

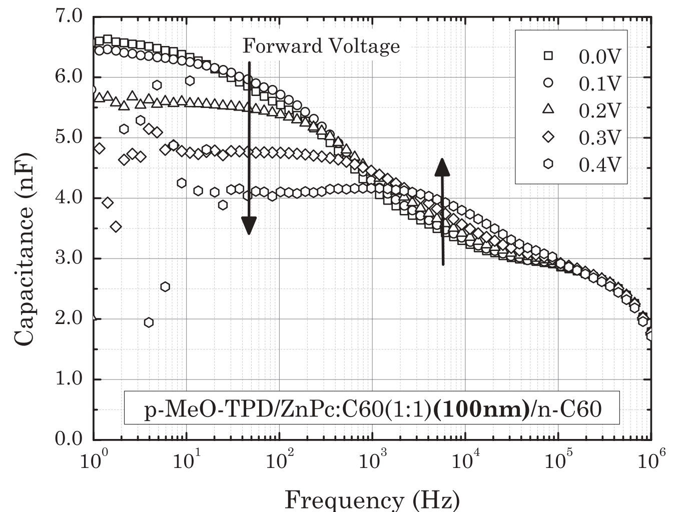

FIG. 10. Measured capacitance spectra of solar cells varying the forward bias voltages. The trap capacitance increases in the moderate frequencies region, because of the lower internal field. The low-frequency range shows a reduced trap contribution due to the trap-assisted recombination.

is possible to observe that the high-frequency plateau (between 10 kHz and 100 kHz) is voltage independent, confirming that no depletion regions, but only the intrinsic layers contribute to the device capacitance in this frequency range. In the low-frequency region, the trap capacitance decreases with increasing reverse voltage, as a consequence of the stronger field in the intrinsic region.

Conversely, when a forward bias is applied to the device, the internal field is reduced and more traps can be populated, as also confirmed by the simulation results of Fig. 9. In particular, not only the number of occupied traps increases, but also the energetic distribution of occupied states is varied. Approaching the flat band condition, also the shallower (or less deep) levels can be populated and contribute to the capacitance. This effect is visible in Fig. 10, for frequencies around 10 kHz.

According to the trapping mechanism proposed in Fig. 4, the trapped electrons are concentrated near the interface with the n-doped transport layer. Far from this surface, the field in the intrinsic layer is able to detrap the electrons that drift back to the doped layer. In Fig. 9, the calculated profile of trapped electrons is shown. Applying a forward bias to the device, the field in the blend layer is reduced and the traps far from the interface with the doped layer are getting populated.

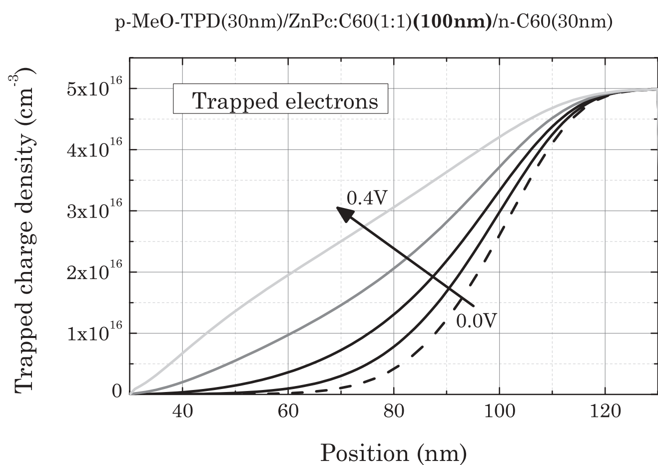

FIG. 9. Simulated density profile of trapped electrons in dark at different (forward) bias voltages. The x axis is confined to the intrinsic layer.

The low-frequency plateau is, however, decreasing with the forward bias. This is no contradiction to the simulation results and the mechanism described by Fig. 4. The explanation is represented by trap-assisted recombination. The application of a forward bias to the device allows for the injection of charge carriers from the contact and a steady-state current flows through the device. In nonequilibrium, two quasi-Fermi levels for electrons and holes can be defined and charge carriers accumulate inside the intrinsic layer. The steady-state current is the result of the balance between charge carrier injection and recombination with the recombination process being more important when the charge carrier density is high. The presence of electrons and holes in the intrinsic layer also enhances the recombination between free and trapped carriers. This effect is not important in the reverse voltage region, because no charge carriers are injected and accumulated in the device. However, in forward bias, charge carriers are injected in the intrinsic layer and recombine with the trapped charges, reducing the amount of trap states that interact with the probe signal. Moreover, energetically different trap states are depopulated with different dynamics. The charge carriers trapped in the deepest states recombine more efficiently with the free carriers and, hence, the trap capacitance is reduced more intensely in the low-frequency region of the capacitance spectra. The response of trap states involved in the recombination process is no more capacitive because they do not store charge carriers anymore. They rather support the current flow in the device, resulting in a resistive behavior. In terms of equivalent circuit, in nonequilibrium conditions the trap states impedance Z_{trap} becomes a resistive element that can be included in the parallel

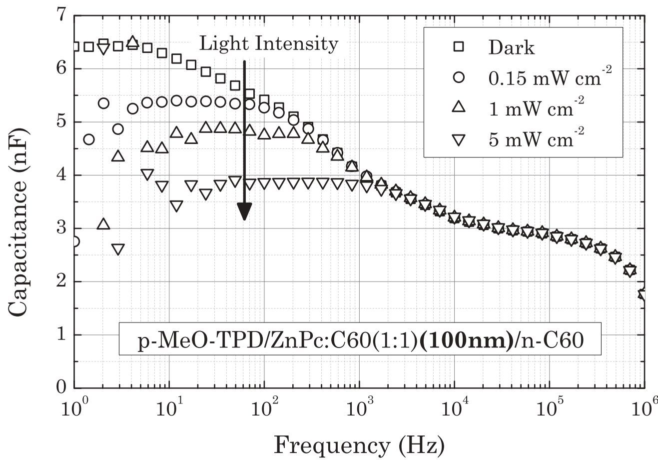

FIG. 11. Measured capacitance spectra of solar cells under light illumination. The presence of photogenerated reduces the plateau at low frequencies, related to the trap capacitance. This behavior confirms that the trap states act as recombination centers.

resistance R_p that now describes both the bimolecular and the trap-assisted recombination.

The dynamics of trapping and detrapping of the trap-assisted recombination is not directly taken into account in the drift-diffusion simulations. The trap states can act as recombination centers but their occupation is statically described by the position of the quasi-Fermi levels.

E. Trap response under illumination

In Fig. 11, the capacitance spectra of a p-i-n solar cell under different illumination intensities are shown. The solar cell is kept at short circuit ($J = J_{sc}$ and $V_{bias} = 0$ V) and the field in the active layer favors charge carrier extraction, with no significant charge accumulation in the intrinsic layer. At these conditions the photogenerated carriers do not significantly perturb the field in the active layer and their main effect is to activate the recombination from trap states, similarly to the application of a forward bias. This effect can be recognized in the capacitance spectrum of Fig. 11. The trap capacitance does not show any increase around 10 kHz, as in Fig. 10, since the internal field and also the population of the shallower trap states is not affected by the illumination.

IV. SUMMARY AND CONCLUSION

In conclusion, trap states are observed in ZnPc:C60 small-molecule solar cells by analyzing the capacitance spectra of the device. The methodology presented in this work leads to a extensive electrical characterization of trap states in small-molecule organic solar cells and is therefore of fundamental importance for the study of any organic device.

Systematic variations in the device structure and in the measuring conditions provide important information about the trap position, occupation mechanism and dynamics. The presence of bulk trap states in the ZnPc:C60 intrinsic active layer is confirmed and it is shown that they have an electron-trapping character. Due to the internal field, only traps close to the interface with the n-doped transport layer are populated and respond to the signal, with the mechanism summarized in Fig. 4. The energetic distribution of the trap states is estimated to be Gaussian with a width of 55 meV, a density of 3.5×10^{16} cm^{-3} and centered 0.458 eV below the C60 electron transport level.

The importance of trap states in the recombination mechanism is demonstrated. It is shown that they are an important aspect to be considered to improve the performance of organic solar cells and more in general organic electronic devices. The electrical model of organic solar cells should include a trap-assisted recombination in presence of a distribution of intragap states, which represents a topic for future work. Further investigations are necessary in order to better understand the origin of the trap states, whether they are morphological defects, impurities characteristic of the fullerene, or defects at the interface between ZnPc and C60 in the blend heterojunction.

ACKNOWLEDGMENTS

This work is supported by the German Federal Ministry of Education and Research (BMBF) in the framework of the OPEG project (13N9720). The authors would like to thank Novaled AG for dopant supply, Debdutta Ray and Wolfgang Tress (IAPP, TU Dresden) for the discussion and the Lesker-team (IAPP, TU Dresden) for the technical support.

[1] T. Kirchartz, B. E. Pieters, J. Kirkpatrick, U. Rau, and J. Nelson, Phys. Rev. B **83**, 115209 (2011).
[2] C. Groves, J. C. Blakesley, and N. C. Greenham, Nano Lett. **10**, 1063 (2010).
[3] G. A. H. Wetzelaer, M. Kuik, H. T. Nicolai, and P. W. M. Blom, Phys. Rev. B **83**, 165204 (2011).
[4] H. T. Nicolai, M. M. Mandoc, and P. W. M. Blom, Phys. Rev. B **83**, 195204 (2011).
[5] M. Kuik, L. J. A. Koster, G. A. H. Wetzelaer, and P. W. M. Blom, Phys. Rev. Lett. **107**, 256805 (2011).
[6] M. M. Mandoc, F. B. Kooistra, J. C. Hummelen, B. de Boer, and P. W. M. Blom, Appl. Phys. Lett. **91**, 263505 (2007).
[7] M. M. Mandoc, B. de Boer, G. Paasch, and P. W. M. Blom, Phys. Rev. B **75**, 193202 (2007).
[8] Y. S. Yang, S. H. Kim, J.-I. Lee, H. Y. Chu, L.-M. Do, H. Lee, J. Oh, T. Zyung, M. K. Ryu, and M. S. Jang, Appl. Phys. Lett. **80**, 1595 (2002).
[9] A. Campbell, D. Bradley, E. Werner, and W. Brütting, Synth. Met. **111-112**, 273 (2000).
[10] J. Simmons and M. Tam, Phys. Rev. B **7**, 3706 (1973).
[11] J. Simmons, G. Taylor, and M. Tam, Phys. Rev. B **7**, 3714 (1973).
[12] P. Stallinga, *Electrical Characterization of Organic Electronic Materials and Devices* (Wiley, Chichester, 2009).
[13] R. D. Pensack, K. M. Banyas, and J. B. Asbury, J. Phys. Chem. C **114**, 5344 (2010).
[14] J. Schafferhans, C. Deibel, and V. Dyakonov, Adv. Energy Mat. **1**, 655 (2011).

[15]R. Schmechel and H. von Seggern, Phys. Status Solidi A **201**, 1215 (2004).
[16]D. Ray, L. Burtone, K. Leo, and M. Riede, Phys. Rev. B **82**, 125204 (2010).
[17]L. Burtone, D. Ray, K. Leo, and M. Riede, J. Appl. Phys. **111**, 064503 (2012).
[18]H. Kleemann, C. Schuenemann, A. A. Zakhidov, M. Riede, B. Lüssem, and K. Leo, Org. Electron. **13**, 58 (2012).
[19]C. Schünemann, D. Wynands, L. Wilde, M. Hein, S. Pfützner, C. Elschner, K.-J. Eichhorn, K. Leo, and M. Riede, Phys. Rev. B **85**, 245314 (2012).
[20]D. Ray, M. Furno, E. Siebert-Henze, K. Leo, and M. Riede, Phys. Rev. B **84**, 075214 (2011).
[21]A. Guerrero, T. Ripolles-Sanchis, P. P. Boix, and G. Garcia-Belmonte, Org. Electron. **13**, 2326 (2012).
[22]M. Riede, T. Mueller, W. Tress, R. Schueppel, and K. Leo, Nanotechnology **19**, 424001 (2008).
[23]B. Maennig, D. Gebeyehu, P. Simon, F. Kozlowski, A. Werner, F. Li, S. Grundmann, S. Sonntag, M. Koch, K. Leo, M. Pfeiffer, H. Hoppe, D. Meissner, N. S. Sariciftci, I. Riedel, V. Dyakonov, J. Parisi, and J. Drechsel, Appl. Phys. A **79**, 1 (2004).
[24]M. Riede, C. Uhrich, J. Widmer, R. Timmreck, D. Wynands, G. Schwartz, W.-M. Gnehr, D. Hildebrandt, A. Weiss, J. Hwang, S. Sundarraj, P. Erk, M. Pfeiffer, and K. Leo, Adv. Funct. Mater. **21**, 3019 (2011).
[25]T. Menke, D. Ray, J. Meiss, K. Leo, and M. Riede, Appl. Phys. Lett. **100**, 093304 (2012).
[26]R. Meerheim, S. Olthof, M. Hermenau, S. Scholz, A. Petrich, N. Tessler, O. Solomeshch, B. Lussem, M. Riede, and K. Leo, J. Appl. Phys. **109**, 103102 (2011).
[27]D. M. Tanenbaum, M. Hermenau, E. Voroshazi, M. T. Lloyd, Y. Galagan, B. Zimmermann, M. Hösel, H. F. Dam, M. Jørgensen, S. A. Gevorgyan, S. Kudret, W. Maes, L. Lutsen, D. Vanderzande, U. Würfel, R. Andriessen, R. Rösch, H. Hoppe, G. Teran-Escobar, M. Lira-Cantu, A. Rivaton, G. Y. Uzunolu, D. Germack, B. Andreasen, M. V. Madsen, K. Norrman, and F. C. Krebs, RSC Advances **2**, 882 (2012).
[28]E. Barsoukov and J. Macdonald, *Impedance Spectroscopy: Theory, Experiment, and Applications* (Wiley, Hoboken, 2005).
[29]J. Bisquert, Phys. Chem. Chem. Phys. **5**, 5360 (2003).
[30]S. Sze and K. K. Ng, *Physics of Semiconductor Devices* (Wiley, Hoboken, 2006).
[31]A. Sanchez-Diaz, L. Burtone, M. Riede, and E. J. Palomares, J. Phys. Chem. C (2012), doi: 10.1021/jp3054422.
[32]See Supplemental Material at http://link.aps.org/supplemental/10.1103/PhysRevB.87.045432.
[33]D. L. Losee, J. Appl. Phys. **46**, 2204 (1975).
[34]J. Bisquert, Phys. Rev. B **77**, 235203 (2008).
[35]J. Bisquert, Phys. Chem. Chem. Phys.: PCCP **10**, 49 (2008).
[36]J. Macdonald and L. Potter, Solid State Ionics **24**, 61 (1987).
[37]W. Tress, K. Leo, and M. Riede, Adv. Funct. Mater. **21**, 2140 (2011).
[38]L. J. A. Koster, V. D. Mihailetchi, and P. W. M. Blom, Appl. Phys. Lett. **88**, 052104 (2006).
[39]W. Shockley and W. Read, Phys. Rev. **87**, 835 (1952).
[40]Y. Zhang, B. de Boer, and P. W. M. Blom, Phys. Rev. B **81**, 85201 (2010).
[41]X. Zhou, J. Blochwitz, M. Pfeiffer, A. Nollau, T. Fritz, and K. Leo, Adv. Funct. Mater. **11**, 310 (2001).
[42]K. Walzer, B. Maennig, M. Pfeiffer, and K. Leo, Chem. Rev. **107**, 1233 (2007).
[43]C. Sah, *Fundamentals of Solid-state Electronics* (World Scientific, Singapore, 1991).